Recent global-warming hiatus tied to equatorial Pacific surface cooling

Yu Kosaka[1] and Shang-Ping Xie[1,2,3]

[1] *Scripps Institution of Oceanography, University of California, San Diego, 9500 Gilman Drive MC 0230, La Jolla, California 92093, USA*

[2] *Physical Oceanography Laboratory and Ocean–Atmosphere Interaction and Climate Laboratory, Ocean University of China, 238 Songling Road, Qingdao, 266100, China*

[3] *International Pacific Research Center, SOEST, University of Hawaii at Manoa, 1680 East West Road, Honolulu, Hawaii 96822, USA*

Despite the continued increase of atmospheric greenhouse gases, the annual-mean global temperature has not risen in this century[1,2], challenging the prevailing view that anthropogenic forcing causes climate warming. Various mechanisms have been proposed for this hiatus of global warming[3-6], but their relative importance has not been quantified, hampering observational estimates of climate sensitivity. Here we show that accounting for recent cooling in the eastern equatorial Pacific reconciles climate simulations and observations. We present a novel method to unravel mechanisms for global temperature change by prescribing the observed history of sea surface temperature over the deep tropical Pacific in a climate model, in addition to radiative forcing. Although the surface temperature prescription is limited to only 8.2% of the global surface, our model reproduces the annual-mean global temperature remarkably well with *r* = 0.97 for 1970-2012 (a period including the current hiatus and an accelerated global warming). Moreover, our simulation captures major seasonal and regional characteristics of the hiatus, including the intensified Walker circulation, the

winter cooling in northwestern and prolonged drought in southern North America. Our results show that the current hiatus is part of natural climate variability, tied specifically to a La Niña-like decadal cooling. While similar decadal hiatus events may occur in the future, multi-decadal warming trend is very likely to continue with greenhouse gas increase.

Daily mean carbon dioxide at Mauna Loa of Hawaii exceeded 400ppm for the first time in May 2013. Whereas the greenhouse gas increase has been shown to cause the centennial trend of global temperature rise since the industrial revolution[7], global temperature has remained flat for the past 15 years (Extended Data Fig. 1). Two schools of idea exist regarding what causes this hiatus of global warming: one suggests a slowdown in radiative forcing due to the stratospheric water vapour[3], the rapid increase of stratospheric and tropospheric aerosols[4,5], and the solar minimum around 2009 (ref. 5), while the other considers the hiatus as part of natural variability, especially a La Niña-like cooling in the tropical Pacific[6]. A quantitative method is necessary to evaluate the relative importance of these mechanisms. Adding to the confusion that, amid the global warming hiatus, record heat waves hit Russia (2010 summer) and US (July 2012), and Arctic sea ice reached record lows (Extended Data Fig. 1). Attributing these regional climate changes requires a dynamic approach. Here we use an advanced climate model that takes radiative forcing and tropical Pacific sea surface temperature (SST) as input. The simulated global-mean temperature is in excellent agreement with observations, showing that the decadal cooling of the tropical Pacific causes the current hiatus. Our dynamic-model based attribution has a distinct advantage over the empirical approach[2,5] by revealing seasonal and regional aspects of the hiatus.

Three sets of experiments were performed based on the Geophysical Fluid Dynamics Laboratory (GFDL) coupled model version 2.1 (CM2.1) (ref. 8). The historical (HIST) experiment is forced with observed atmospheric composition changes

and the solar cycle. In Pacific Ocean-Global Atmosphere (POGA) experiments, SST anomalies in the equatorial eastern Pacific (8.2% of the Earth surface) follow the observed evolution (see Methods). In POGA-H, the radiative forcing is identical to HIST, while in the POGA control experiment (POGA-C) it is fixed at 1990 value. Outside the equatorial eastern Pacific, the atmosphere and ocean are fully coupled and free to evolve.

Figure 1 compares the observed and simulated global near-surface temperature. In HIST, the annual-mean temperature keeps rising in response to the increased radiative forcing, with expanding departures from observations for the recent decade (Fig. 1a). POGA-H well reproduces the observed record (Extended Data Table 1). For a 43-year period after 1970 when equatorial Pacific SST data are more reliable, correlation (r) with observations is $r = 0.97$ for POGA-H, due largely to the long-term trend ($r = 0.90$ for HIST). Detrended, POGA-H still reproduces the observations at $r = 0.70$, whereas it falls to 0.26 in HIST. POGA-C illustrates the tropical control of the global temperature with constant radiative forcing, with the global-mean temperature closely following tropical Pacific variability (Fig. 1b). The global-mean surface air temperature (SAT) changes by 0.29ºC in response to a 1ºC SAT anomaly over the equatorial eastern Pacific. For the recent decade, the decrease in tropical Pacific SST has lowered the global temperature by ~0.15°C compared to the 1990s (Fig. 1b), opposing the radiative forcing effect and causing the hiatus. Likewise an El Niño-like trend in the tropics[9] accelerated the global warming from the 1970s to late 1990s[10] (Extended Data Table 1).

The POGA experimental design has been used to study global teleconnections of interannual El Niño-Southern Oscillation (ENSO)[11,12]. Here we have presented a novel application of POGA and demonstrated its skill in simulating the observed decadal modulations of the global warming trend including the peculiar hiatus. Our results show that the two-parameter (radiative forcing and tropical Pacific SST) system is remarkably

skilful in reproducing the observed global-mean temperature record, superior over the HIST results with radiative forcing alone. In individual HIST realizations, hiatus events feature decadal La Niña-like cooling in the tropical Pacific[6] (Extended Data Fig. 2), but POGA-H enables a direct year-by-year comparison with the observed timeseries of global temperature, not just the statistics from unconstrained coupled runs.

We focus on trends over the recent 11 years from 2002 to 2012, to avoid the strong 1997/98 El Niño event and the following 3-year La Niña events. Net downward radiation and ocean heat content in POGA-H have continued to increase during the global SAT hiatus[6] (Extended Data Fig. 3). The SAT hiatus is confined to the cold season[13] (referred to the boreal seasons hereafter), with a decadal cooling trend for November-April, while the global temperature continues to rise during summer (Fig. 1c). POGA-H reproduces this seasonal cycle of the hiatus, albeit with a somewhat reduced amplitude. Although the La Niña-like cooling trend in the tropical Pacific is similar between winter and summer (Extended Data Fig. 4a), stationary/transient eddies, the dominant mechanism for meridional heat transport[14], are stronger in winter than summer. As a result, the tropical cooling effect on the extratropics is most pronounced in winter (seasonality of the temperature trend in the Southern Hemisphere extratropics is weak). The tropical influence on the Northern Hemisphere (NH) extratropics is weak during the summer, allowing the radiative forcing to continue the warming trend during the recent decade (Extended Data Fig. 4b).

This seasonal contrast is evident also in HIST. For 1970-2040, a period when the ensemble-mean global temperature shows a steady increase in HIST, the probability density function (PDF) for 11-year trend is similar between winter and summer for tropical temperature, with means both around 0.25°C (Extended Data Fig. 4c). The PDF is much broader for winter than summer for NH extratropical temperature (Extended Data Fig. 4d). The chance for 11-year temperature change to fall below -0.3°C is 8% for

winter but only 0.7% for summer in the NH extratropics (~4% in the tropics for both seasons). The 11-fold increase in the chance of an extratropical cooling in winter is due partly to the stronger tropical influence than in summer.

We examine regional climate change associated with the hiatus. While models project a slowdown of the Walker circulation in global warming[15], the Pacific Walker cell intensified during the past decade (Fig. 2c). POGA-H captures this circulation change, forced by the SST cooling across the tropical Pacific (Fig. 2d). As in interannual ENSO, the tropical Pacific cooling excites global teleconnections in December-January-February (DJF; the season is denoted with first letters of the months). SST changes in POGA-H are in broad agreement with observations over the Indian Ocean, South Atlantic, and Pacific outside the restoring domain (Figs. 2a,b). The model reproduces the weakening of the Aleutian low as the response of the Pacific-North American pattern to tropical Pacific cooling[11] (Figs. 2c,d). As a result, the SAT change over North America is well reproduced, including a pronounced cooling in the northwestern continent. The model fails to simulate the SAT and sea-level pressure (SLP) changes over Eurasia, suggesting that they are due to internal variability unrelated to tropical forcing (Extended Data Fig. 5, left panels).

In summer, the broad agreement between simulated and observed SST remains over the Pacific (Figs. 3a,b) but the tropical influence on SAT over extratropical Eurasia and Arctic is weak (Extended Data Fig. 5, right panels), and the increasing radiative forcing permits heat waves to develop in NH continents and Arctic sea ice to melt. (The model does not produce the record shrinkage of Arctic sea ice because of model biases and natural variability in the Arctic.) We note that the observed JJA warming in western midlatitude Eurasia is much more intense than in POGA-H as heat waves there (2003 in central Europe and 2010 in Russia) are associated with long-lasting blocking events unrelated to tropical variability[16]. POGA-H captures the rainfall decrease and warming

over the southern US, changes associated with prolonged droughts of record severity in Texas[17]. The southern US anomalies are probably tropical-forced (Extended Data Fig. 5, right panels), for which winter-spring precipitation deficits and land-surface memory processes are likely important[17]. Likewise, during the epoch of accelerated global warming from the 1970s to late 1990s, the southern US appears as a warming hole[18], a spatial pattern likely tied to tropical SST (Extended Data Fig. 6).

We have presented a unique dynamic-based method for quantitative attributions of decadal modulations of global warming. By prescribing observed SST in only 8.2% of the Earth's surface, POGA-H reproduces the observed timeseries of global-mean temperature strikingly well, including interannual to decadal variability. The comparison between HIST and POGA-H indicates that the decadal cooling of the tropical Pacific is the culprit of the current hiatus. In addition, POGA-H reproduces the seasonal and key regional patterns of the hiatus. The La Niña-like cooling in the tropics affects the extratropics strongly in boreal winter, causing a global cooling, weakened Aleutian low, and enhanced cooling over northwestern North America among other regional anomalies. In boreal summer, by contrast, the NH extratropics is largely shielded from the tropical influence, and the temperature continues to rise in response to the increased radiative forcing.

A question remains whether the La Niña-like decadal trend is internal or forced. We note the following facts: i) The tropical Pacific features pronounced low-frequency SST variability (Extended Data Fig. 7), so large that the pattern of modest forced response has yet emerged from observations (Fig. 1b). ii) All the climate models project a tropical Pacific warming in response to increased greenhouse gas concentrations[7]. We conclude that the recent cooling of the tropical Pacific and hence the current hiatus are likely due to natural internal variability rather than a forced response. As such, the hiatus is temporary, and global warming will return when the tropical Pacific swings

back to a warm state. Similar hiatus events may occur in the future and are difficult to predict at multi-year leads due to limited predictability of tropical Pacific SST. We showed that when taking place, such events are accompanied by characteristic regional patterns including an intensified Walker circulation, weakened Aleutian low and prolonged droughts in the southern US.

While radiative-forced response will become increasingly important, deviations from the forced response are substantial at any given time, especially on regional scales[19]. Quantitative tools like our POGA-H are crucial to attribute the causes of regional climate anomalies[17]. The current hiatus illustrates the global influence of tropical Pacific SST, and a dependency of climate sensitivity on the spatial pattern of tropical ocean warming, which itself is uncertain in observations[20] and among models[21,22]. This highlights the need to develop predictive pattern dynamics constrained by observations.

Methods summary

We use the Hadley Centre-Climate Research Unit combined land SAT and SST (HadCRUT) version 4.1.1.0 (ref. 23), the Hadley Centre mean SLP dataset version 2 (HadSLP2, ref. 24) and monthly precipitation data from Global Precipitation Climatology Project (GPCP) version 2.2 (ref. 25). We examine three sets of coupled model experiments based on GFDL CM2.1 (ref. 8). HIST is forced by historical radiative forcing for 1861-2005 and Representative Concentration Pathway 4.5 (RCP4.5) for 2006-2040, based on Coupled Model Intercomparison Project phase 5 (CMIP5, ref. 26). In POGA-H and POGA-C experiments, SST is restored to the model climatology plus historical anomaly by a Newtonian cooling over the deep tropical eastern Pacific. The restoring timescale is 10 days for a 50 m mixed layer. Figures 2b and 3b shows the region where SST is restored; within the inner box the ocean surface heat flux is fully overridden, while in the buffer zone between the inner and outer boxes, the flux is blended with the model-diagnosed one. In POGA-H, radiative forcing is identical to HIST, while it is fixed at 1990 values in POGA-C. The three experiments consist of 10 member runs each.

References

1. Easterling, D. R. & Wehner, M. F. Is the climate warming or cooling? *Geophys. Res. Lett.* **36**, L08706 (2009).
2. Foster, G. & Rahmstorf, S. Global temperature evolution 1979-2010. *Environ. Res. Lett.* **6**, 044022, doi:10.1088/1748-9326/6/4/044022 (2011).
3. Solomon, S. *et al.* Contributions of stratospheric water vapor to decadal changes in the rate of global warming. *Science* **327**, 1219–1223 (2010).
4. Solomon, S. *et al.* The persistently variable "background" stratospheric aerosol layer and global climate change. *Science* **333**, 866–870 (2011).
5. Kaufmann, R. K., Kauppi, H., Mann, M. L. & Stock, J. H. Reconciling anthropogenic climate change with observed temperature 1998-2008. *Proc. Natl. Acad. Sci. USA* **108**, 11790–11793 (2011).
6. Meehl, G. A., Arblaster, J. M., Fasullo, J. T., Hu, A. & Trenberth, K. E. Model-based evidence of deep-ocean heat uptake during surface-temperature hiatus periods. *Nature Clim. Change* **1**, 360–364 (2011).
7. Meehl, G. A. *et al.* in *Climate Change 2007: The Physical Science Basis* (eds. Solomon, S. *et al.*). 747–845 (Cambridge University Press, 2007).
8. Delworth, T. L. *et al.* GFDL's CM2 global coupled climate models. Part I: Formulation and simulation characteristics. *J. Clim.* **19**, 643–674 (2006).
9. Zhang, Y., Wallace, J. M. & Battisti, D. S. ENSO-like interdecadal variability: 1900–93. *J. Clim.* **10**, 1004–1020 (1997).
10. Meehl, G. A., Hu, A., Arblaster, J., Fasullo, J. & Trenberth, K. E. Externally forced and internally generated decadal climate variability associated with the Interdecadal Pacific Oscillation. *J. Clim.*, doi: 10.1175/JCLI-D-12-00548.1 (in press).
11. Alexander, M. A. *et al.* The atmospheric bridge: The influence of ENSO teleconnections on air-sea interaction over the global oceans. *J. Clim.* **15**, 2205–2231 (2002).
12. Lau, N.-C. & Nath, M. J. The role of the "atmospheric bridge" in linking tropical Pacific ENSO events to extratropical SST anomalies. *J. Clim.* **9**, 2036–2057 (1996).

13. Cohen, J. L., Furtado, J. C., Barlow, M., Alexeev, V. A. & Cherry, J. E. Asymmetric seasonal temperature trends. *Geophys. Res. Lett.* **39**, L04705 (2012).
14. Trenberth, K. E., Caron, J. M., Stepaniak, D. P. & Worley, S. Evolution of El Niño-Southern Oscillation and global atmospheric surface temperatures. *J. Geophys. Res.* **107**, AAC 5-1–AAC 5-17 (2002).
15. Vecchi, G. A. *et al.* Weakening of tropical Pacific atmospheric circulation due to anthropogenic forcing. *Nature* **441**, 73–76 (2006).
16. Barriopedro, D., Garcia-Herrera, R., Lupo, A. R. & Hernandez, E. A climatology of northern hemisphere blocking. *J. Clim.* **19**, 1042–1063 (2006).
17. Hoerling, M. *et al.* Anatomy of an extreme event. *J. Clim.* **26**, 2811–2832 (2013).
18. Wang, H. *et al.* Attribution of the seasonality and regionality in climate trends over the United States during 1950-2000. *J. Clim.* **22**, 2571–2590 (2009).
19. Deser, C., Knutti, R., Solomon, S. & Phillips, A. S. Communication of the role of natural variability in future North American climate. *Nature Clim. Change* **2**, 775–779 (2012).
20. Tokinaga, H., Xie, S.-P., Deser, C., Kosaka, Y. & Okumura, Y. M. Slowdown of the Walker circulation driven by tropical Indo-Pacific warming. *Nature* **491**, 439–443 (2012).
21. DiNezio, P. N., Clement, A. C., Vecchi, G. A., Soden, B. J. & Kirtman, B. P. Climate response of the equatorial Pacific to global qarming. *J. Clim.* **22**, 4873–4892 (2009).
22. Ma, J. & Xie, S.-P. Regional patterns of sea surface temperature change: A source of uncertainty in future projections of precipitation and atmospheric circulation. *J. Clim.* **26**, 2482–2501 (2013).
23. Morice, C. P., Kennedy, J. J., Rayner, N. A. & Jones, P. D. Quantifying uncertainties in global and regional temperature change using an ensemble of observational estimates: The HadCRUT4 data set. *J. Geophys. Res.* **117**, D08101 (2012).
24. Allan, R. & Ansell, T. A new globally complete monthly historical gridded mean sea level pressure dataset (HadSLP2): 1850-2004. *J. Clim.* **19**, 5816–5842 (2006).

25. Adler, R. F. *et al.* The version-2 global precipitation climatology project (GPCP) monthly precipitation analysis (1979-present). *J. Hydrometeorol.* **4**, 1147–1167 (2003).

26. Taylor, K. E., Stouffer, R. J. & Meehl, G. A. An overview of CMIP5 and the experiment design. *Bull. Am. Meteorol. Soc.* **93**, 485–498 (2012).

Acknowledgements. We wish to thank GFDL model developers for making CM2.1 available; L. Xu, Y. Du, N. C. Johnson and C. Deser for discussions. The work was supported by NSF (ATM-0854365), the National Basic Research Program of China (2012CB955600), and NOAA (NA10OAR4310250).

Author Contributions. Y.K. and S.-P.X. designed the model experiments. Y.K. performed the experiments and analysis. S.-P.X. and Y.K. wrote the manuscript.

Author Information. The authors declare no competing financial interests. Correspondence and requests for materials should be addressed to S.-P.X. (sxie@ucsd.edu).

Figure legends

Figure 1. Observed and simulated global temperature trends. Annual-mean timeseries based on **a,** observations, HIST and POGA-H; and **b,** POGA-C. Anomalies are deviations from the 1980-1999 averages, except for HIST, for which the reference is the 1980-1999 average of POGA-H. SAT anomalies over the restoring region are plotted in **b**, with the axis on the right. Major volcanic eruptions are indicated in **a**. **c,** Trends of seasonal global temperature for 2002-2012 in observations and POGA-H. Shading represents 95% confidence interval of ensemble means. Bars on the right of **a** show ranges of ensemble spreads of the 2002-2012 averages.

Figure 2. Observed and simulated trend patterns in boreal winter for 2002-2012. **a-b,** Near-surface temperature, and **c-d**, SLP, from observations (left panels) and POGA-H (right panels) in DJF. Grey shading represent missing values. Stippling indicate regions exceeding 95% statistical confidence. Purple boxes in **b** show the restoring region of POGA experiments.

Figure 3. Observed and simulated trend patterns in boreal summer for 2002-2012. Same as Fig. 2, but **a-b**, near-surface temperature and **c-d**, precipitation in JJA.

Methods

Gridded observational datasets. We use the Hadley Centre-Climate Research Unit combined land SAT and SST (HadCRUT) version 4.1.1.0 (http://www.metoffice.gov.uk/hadobs/crutem4/; ref. 23); the Hadley Centre mean SLP dataset version 2 (HadSLP2, http://www.metoffice.gov.uk/hadobs/hadslp2/; ref. 24); monthly precipitation data from Global Precipitation Climatology Project (GPCP) version 2.2 (http://www.gewex.org/gpcp.html; ref. 25). HadCRUT is compared with SAT of the model.

Model experiments. We use GFDL CM2.1 (ref. 8). HIST, POGA-H and POGA-C experiments are made of 10 member runs each. HIST is forced by historical radiative forcing of the Coupled Model Intercomparison Project phase 5 (CMIP5, ref. 26) for 1861-2005 and extends to 2040 with Representative Concentration Pathway 4.5 (RCP4.5). The forcing includes greenhouse gases, aerosols, ozone, the solar activity cycle (repeating the cycle for 1996-2008 after 2009) and land use.

In POGA experiments, deep tropical eastern Pacific SST is restored to the model climatology plus historical anomaly, by overriding surface sensible heat flux to ocean ($F^{\downarrow}$) with

$$F^{\downarrow} = (1-\alpha)F_*^{\downarrow} + \alpha(cD/\tau)\cdot\left(T' - T_*'\right).$$

Here the prime indicates the anomaly, asterisks represent model-diagnosed values, and T denotes SST. The reference temperature anomaly T' is based on Hadley Centre Ice and SST version 1 (HadISST1, http://www.metoffice.gov.uk/hadobs/hadisst/; ref. 27). The model anomaly is the deviation from the climatology of a 300-year control experiment. c is the specific heat of sea water, D = 50 m the typical depth of the ocean-mixed layer, and τ = 10 d is the restoring timescale. Figures 2b and 3b show the

region where SST is restored: $\alpha = 1$ within the inner box, linearly reduced to zero in the buffer zone from the inner to the outer boxes. In POGA-H, radiative forcing is identical to HIST, while it is fixed at 1990 values in POGA-C.

Trend estimates. Trends are calculated as the Sen median slope[28]. For observed surface temperature, trends are calculated for grid boxes where data are available for > 80% of years with at least one month per season. Mann-Kendall test is performed for statistical significance of trends shown in Figs. 2, 3 and Extended Data Fig. 6, while *t*-test is applied for significance of composited differences/anomalies of trends (Extended Data Table 1 and Extended Data Fig. 2). In Extended Data Figs. 4c,d, the trends are evaluated every 4 years for individual members of HIST, and PDFs are plotted with a kernel density estimation and a Gaussian smoother.

Decadal variability. In Extended Data Figs. 5 and 7, Lanczos low-pass filter with a half-power frequency of 8 years has been applied to extract decadal variability. Extended Data Fig. 5 shows decadal anomalies obtained from a regression analysis, with their statistical significance tested with *t*-statistic.

Other observational datasets. For Extended Data Fig. 1, we also use the Southern Oscillation Index (http://www.cpc.ncep.noaa.gov/data/indices/; ref. 29) and US National Snow and Ice Data Center Arctic sea ice extent (http://nsidc.org/data/seaice_index/; ref. 30).

27. Rayner, N. A. *et al.* Global analyses of sea surface temperature, sea ice, and night marine air temperature since the late nineteenth century. *J. Geophys. Res.* **108**, 4407 (2003).

28. Sen, P. K. Estimates of regression coefficient based on Kendall's tau. *J. Am. Stat. Assoc.* **63**, 1379–1389 (1968).

29. Trenberth, K. E. Signal versus noise in the Southern Oscillation. *Mon. Wea. Rev.* **112**, 326–332 (1984).

30. Fetterer, F. & Knowles, K. Sea ice index monitors polar ice extent. *Eos* **85**, 163 (2004).

Title and Legend for Extended Data Table

Extended Data Table 1. Evaluation of simulations of observed global mean temperature and its trend

All based on ensemble-mean values. Correlations and root mean square errors are evaluated for 1970-2012 with respect to observations. The trends are significantly different between the experiments at $P < 0.01$ (2002-2012) and $P < 0.05$ (1971-1997) based on *t*-test applied for the ensembles.

Legends for Extended Data figures

Extended Data Figure 1. Observed climate indices for the recent decade. (From top to bottom) Annual-mean global near-surface temperature anomalies from the 1980-1999 average, DJF Southern Oscillation Index, DJF SLP near Aleutian Islands (40º-60ºN, 170º-120º W), JJA SAT over the US (30º-45ºN, 110º-80ºW), and September Arctic sea ice extent.

Extended Data Figure 2. 11-year trends of annual-mean SAT composited for 34 hiatus events in HIST. The hiatus events are chosen for which annual-mean global SAT trends are smaller than their ensemble mean minus 0.3 ºC per 11 yr. Stippling indicates 95% statistical confidence. Note that a typical hiatus in HIST features a La Niña-like pattern in the tropics and SST cooling around the Aleutian Islands, patterns similar to the current hiatus event.

Extended Data Figure 3. Net radiative imbalance and ocean heat content increase in POGA-H and HIST. a-b, Net radiative imbalance at the top-of-atmosphere. Positive values indicate net energy flux into the planet. **c-d,** Ocean heat content deviations from

1950 values for each ensemble member. POGA-H (left panels) and HIST (right panels). Shading represents 95% confidence interval of ensemble means. Major volcanic eruptions are indicated. The radiative imbalance has remained positive and ocean heat content has kept increasing for the recent decade in both of the experiments. Note that the energy budget is not closed in POGA.

Extended Data Figure 4. Seasonal dependency of regional temperature trends. a-b Observed temperature anomalies (solid) and their trends (dashed) for the recent decade (ºC). **c-d** PDFs (curves) and means (vertical lines) of 11-year SAT trends in HIST for 1971-2040. Temperature has been averaged over the tropics (20ºS-20ºN; left panels) and the northern extratropics (20º-90ºN; right panels) for JJA (red) and DJF (blue). Note that the northern extratropics features a larger PDF spread in winter than summer, in contrast to a high similarity in the tropics. The winter spread is also greater in the extratropics than the tropics, whereas the opposite is true for summer.

Extended Data Figure 5. Decadal anomalies associated with SST cooling over the equatorial Pacific. Low-pass filtered inter-member anomalies in HIST regressed against SST anomalies over [5ºS-5ºN, 170ºE-130ºW] (white boxes in **a,b**). **a-b,** SAT, **c-d**, SLP and **e-f**, precipitation for DJF (left panels) and JJA (right panels). The sign is flipped to show a La Niña state. Stippling indicates 95% statistical confidence. Note that cold anomalies spread to the Arctic region in boreal winter but are restricted south of 60ºN in summer. Anomalies in the tropics, the North Pacific and North America are broadly consistent with the trends for the current hiatus.

Extended Data Figure 6. Observed and simulated trend patterns in boreal summer for the accelerated global warming period. a-b, Temperature and **c-d**, precipitation from observations (left panels) and POGA-H (right panels) in JJA. **a,b,d,** Trends for 1971-1997, and **c,** trend is evaluated for 1979-1997 and scaled to 27-year change.

Stippling indicates 95% statistical confidence. Purple boxes in **b** show the restoring region of POGA experiments. Note the widespread warming, with weak cooling in the North and South Pacific and a weakened Walker circulation. POGA-H reproduces warming hole[18] (warming minimum/cooling in the central US) with slight geographical displacements due to model biases.

Extended Data Figure 7. Internal decadal variability in SST. Standard deviations of annual-mean SST from **a,** observations[27] detrended for 1900-2012 and **b,** inter-member anomalies in HIST. Evaluated with a decadal low-pass filter. Note that tropical variance is most pronounced in the Pacific.

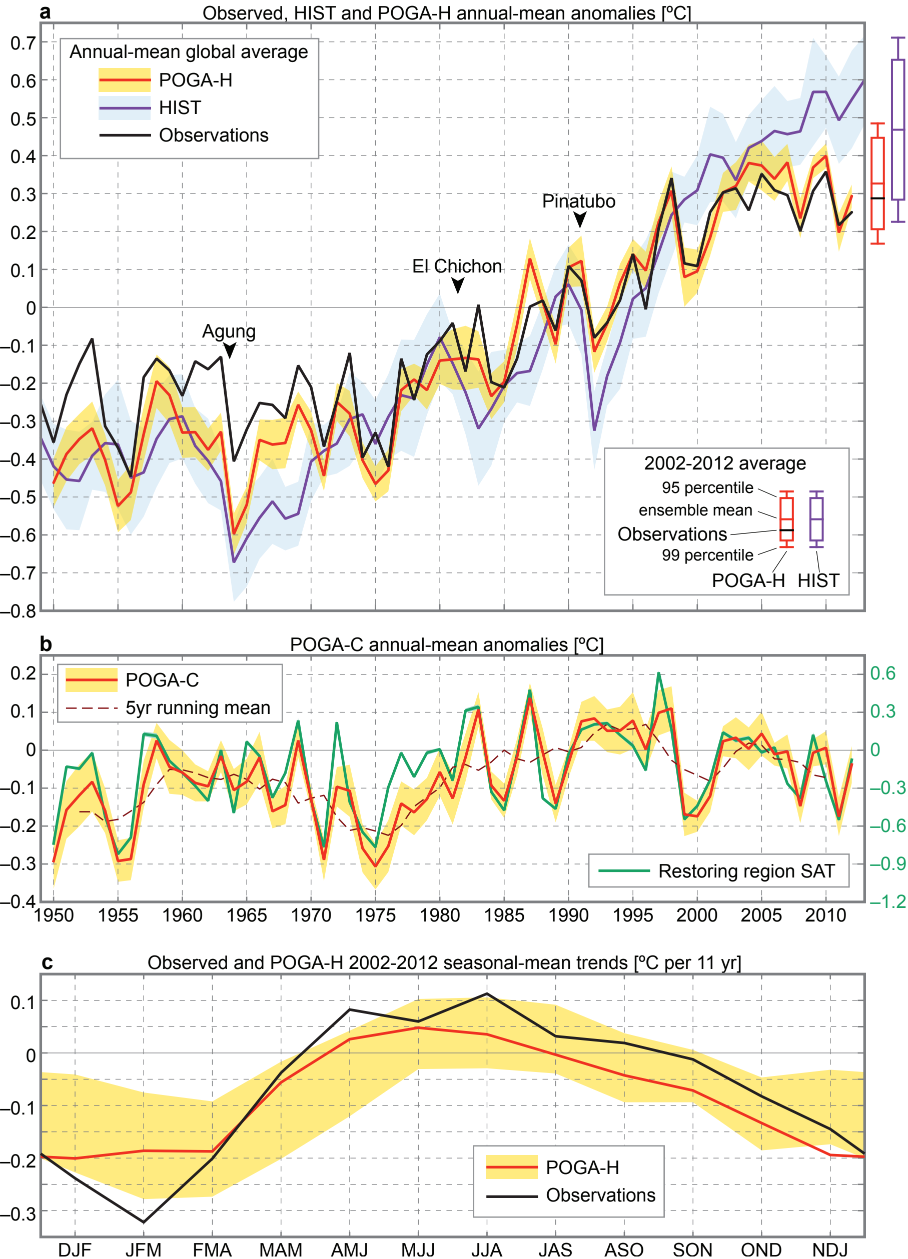

a
Observed, HIST and POGA-H annual-mean anomalies [ºC]
Annual-mean global average
POGA-H
HIST
Observations
Agung
El Chichon
Pinatubo
2002-2012 average
95 percentile
ensemble mean
Observations
99 percentile
POGA-H
HIST
b
POGA-C annual-mean anomalies [ºC]
POGA-C
5yr running mean
Restoring region SAT
c
Observed and POGA-H 2002-2012 seasonal-mean trends [ºC per 11 yr]
POGA-H
Observations
DJF
JFM
FMA
MAM
AMJ
MJJ
JJA
JAS
ASO
SON
OND
NDJ

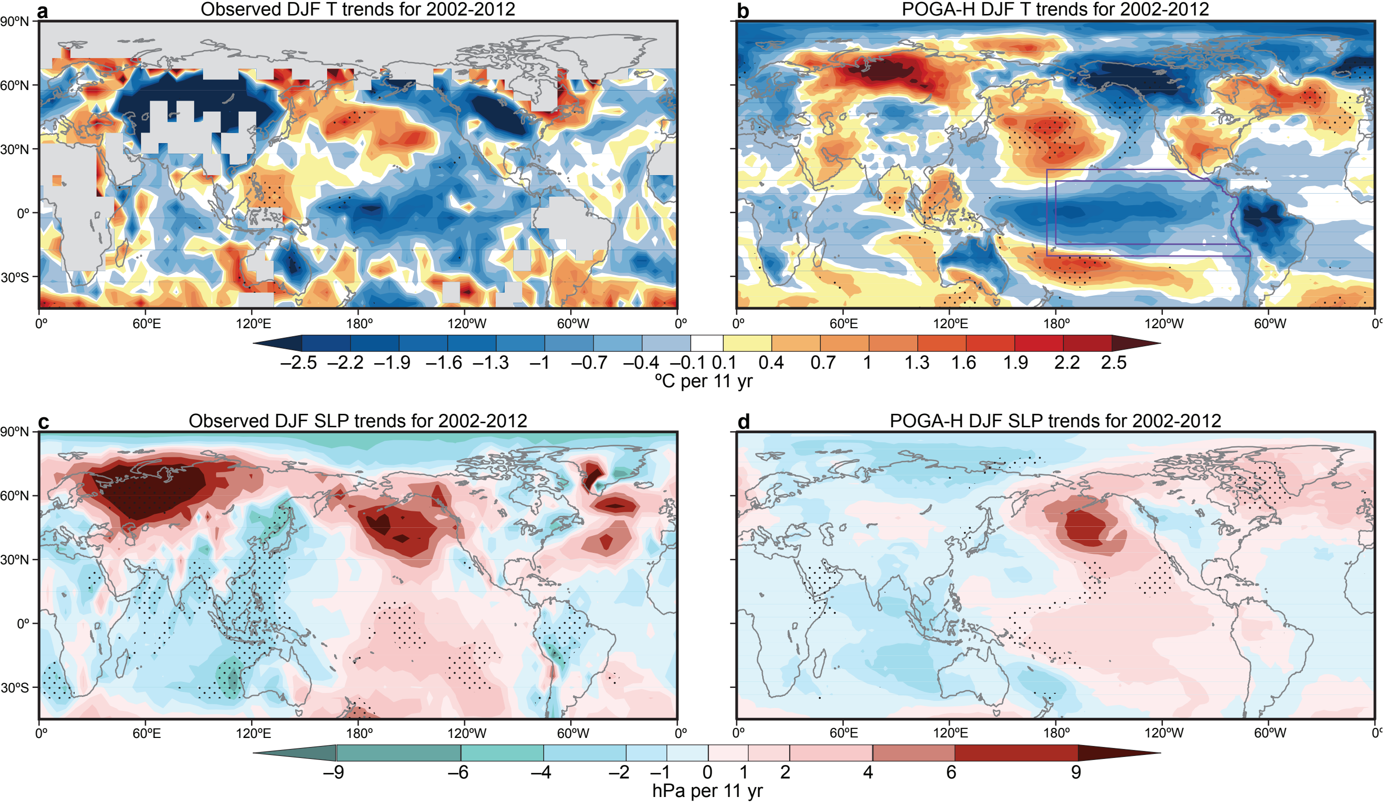

a
Observed DJF T trends for 2002-2012
b
POGA-H DJF T trends for 2002-2012
90ºN
60ºN
30ºN
0º
30ºS
0º
60ºE
120ºE
180º
120ºW
60ºW
−2.5 −2.2 −1.9 −1.6 −1.3 −1 −0.7 −0.4 −0.1 0.1 0.4 0.7 1 1.3 1.6 1.9 2.2 2.5
ºC per 11 yr
c
Observed DJF SLP trends for 2002-2012
d
POGA-H DJF SLP trends for 2002-2012
−9 −6 −4 −2 −1 0 1 2 4 6 9
hPa per 11 yr

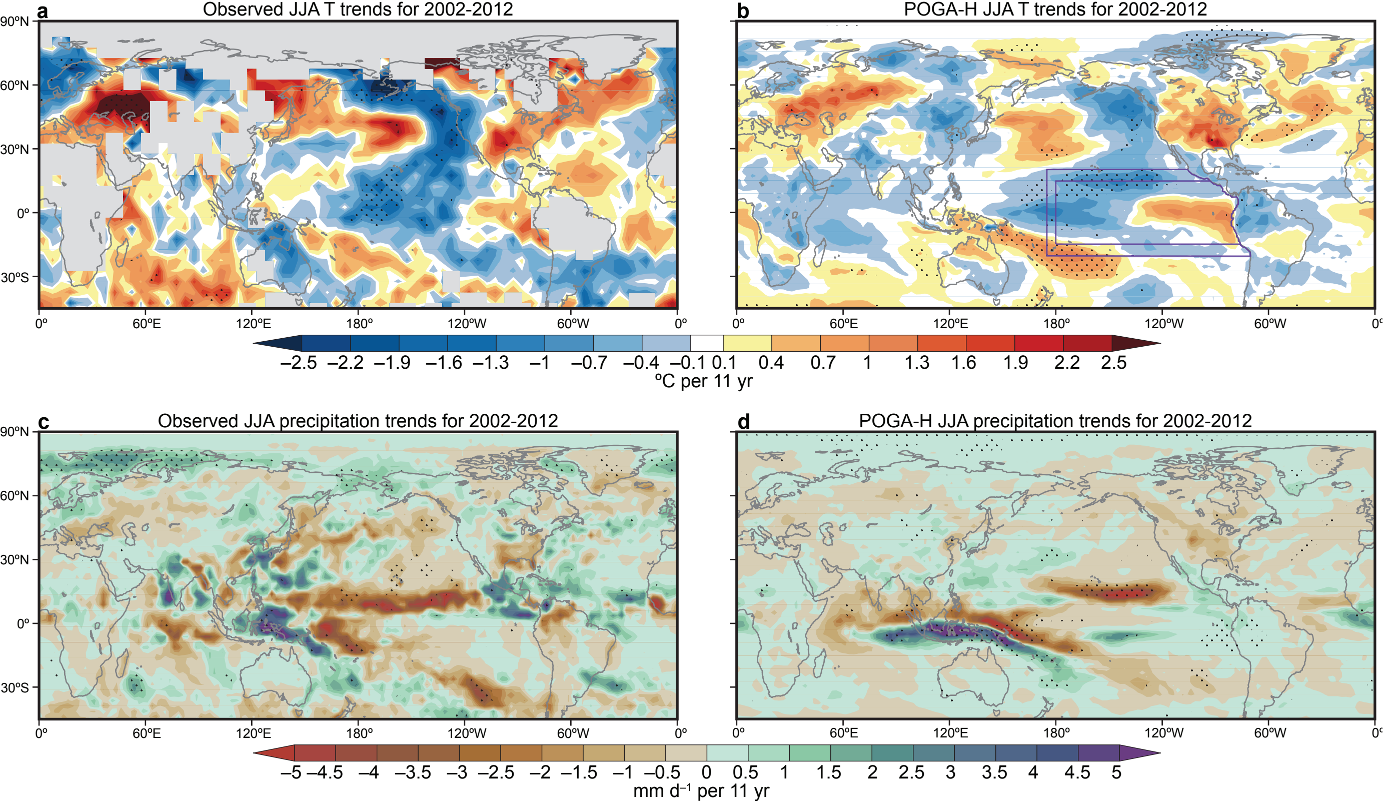

a
Observed JJA T trends for 2002-2012
b
POGA-H JJA T trends for 2002-2012
90ºN
60ºN
30ºN
0º
30ºS
0º
60ºE
120ºE
180º
120ºW
60ºW
−2.5 −2.2 −1.9 −1.6 −1.3 −1 −0.7 −0.4 −0.1 0.1 0.4 0.7 1 1.3 1.6 1.9 2.2 2.5
ºC per 11 yr
c
Observed JJA precipitation trends for 2002-2012
d
POGA-H JJA precipitation trends for 2002-2012
−5 −4.5 −4 −3.5 −3 −2.5 −2 −1.5 −1 −0.5 0 0.5 1 1.5 2 2.5 3 3.5 4 4.5 5
mm d−1 per 11 yr